Combustion Theory and Modelling
Publication details, including instructions for authors and subscription information:
http://www.tandfonline.com/loi/tctm20

Experimental and numerical study of probe-induced perturbations of the flame structure

P.A. Skovorodko [a], A.G. Tereshchenko [b], O.P. Korobeinichev [b], D.A. Knyazkov [b] & A.G. Shmakov [b]

[a] Department of Rarefied Gases, Kutateladze Institute of Thermophysics, Novosibirsk, 630090, Russia

[b] Laboratory of Kinetics of Combustion Processes, Institute of Chemical Kinetics and Combustion, Novosibirsk, 630090, Russia

Version of record first published: 02 Nov 2012.

To cite this article: P.A. Skovorodko , A.G. Tereshchenko , O.P. Korobeinichev , D.A. Knyazkov & A.G. Shmakov (2013): Experimental and numerical study of probe-induced perturbations of the flame structure, Combustion Theory and Modelling, 17:1, 1-24

To link to this article: http://dx.doi.org/10.1080/13647830.2012.715674

Combustion Theory and Modelling, 2013
Vol. 17, No. 1, 1–24, http://dx.doi.org/10.1080/13647830.2012.715674

Experimental and numerical study of probe-induced perturbations of the flame structure

P.A. Skovorodko[a], A.G. Tereshchenko[b*], O.P. Korobeinichev[b], D.A. Knyazkov[b] and A.G. Shmakov[b]

[a]*Department of Rarefied Gases, Kutateladze Institute of Thermophysics, Novosibirsk, 630090, Russia;* [b]*Laboratory of Kinetics of Combustion Processes, Institute of Chemical Kinetics and Combustion, Novosibirsk, 630090, Russia*

(*Received 7 February 2012; final version received 18 July 2012*)

A study is made of the external flow of an atmospheric-pressure burner-stabilised methane-oxygen-argon flame near an axisymmetric conical sampling probe with an orifice at the centre of the cone tip. The flow is simulated by solving the full set of unsteady Navier-Stokes equations using a recently developed original algorithm. Heat release due to chemical reactions is approximately described by a source term in the energy equation which provides a given temperature distribution in the unperturbed isobaric flame. On the probe orifice surface, the axial gas velocity is assumed to be equal to the local velocity of sound. A qualitative understanding of the nature and magnitude of the perturbing effects of the probe on the flame is obtained by comparing the steady flow near the probe and the unperturbed flame. Probe-induced distortions in the flame mixture composition are simulated by calculating concentration distributions of some species (CH_4, CO_2, H_2O, and O_2) in the flow field from the diffusion equation for binary gas mixtures (CH_4 – Ar, CO_2 – Ar, etc.) in a linear formulation. The effect of chemical reactions is approximately described by a source term in the diffusion equation which provides given concentration distributions in the unperturbed flame. The developed approach based on spatially fixed sources of energy and species concentrations provides more realistic simulations of probe-induced perturbations of the flame structure than the approaches described in the literature. The data demonstrating the nature of the probe-perturbed flame under conditions close to real ones were obtained for the first time.

Keywords: mass-spectrometry sampling; simulation; flame structure; perturbation; shift

Nomenclature

c_0	speed of sound on burner surface
c_i	mass fraction of species i (i = 1, 2)
d	diameter of the probe orifice
D_{12}	binary diffusion coefficient
dy	mesh size in radial direction
dz	mesh size in axial direction
e	specific internal energy
h_0	unit used for linear variables

*Corresponding author. Email: tereshag@kinetics.nsc.ru

G gas flow rate
k_T thermal diffusion ratio
m mean molecular weight of binary mixture
m_i molecular weight of species i (i = 1, 2)
n number density
p pressure
Pr Prandtl number
Q_T source term for energy equation
Q_c source term for diffusion equation
R gas constant
Re Reynolds number
Sc Schmidt number
t time
T temperature
u radial component of the total velocity
w axial component of the total velocity
y radial coordinate
z axial coordinate
z_0 distance from the burner to the probe

Greek

α probe sampling factor
δ shift of concentration profiles
ε, σ parameters of the Lennard-Jones (6–12) potential
ε_T emissivity
κ specific heat ratio
λ heat conductivity
μ dynamic viscosity
μ' bulk viscosity
ν parameter determining the flow with plane or axial types of symmetry
ρ mass density
φ equivalence ratio

Subscript

0 parameters on burner surface

Symbols

$\sim$ over a symbol denotes dimensionless variables

1. Introduction

Mass spectrometric sampling is one of the most important methods of flame diagnostics. Two types of sampling apparatus are used to study the flame structure. The sample is transported to the ion source in the form of (1) a molecular flow using a microprobe – a cone with an opening angle of 5–20 degrees and an inlet orifice of 5–20 μm, and (2) a molecular beam using a "sonic" probe with a cone angle equal to, or greater than, 40 degrees and an inlet orifice of 20–300 μm and a skimmer. Microprobes have high spatial resolution and disturb the flame only slightly, but radicals and unstable species, including vapour, can recombine. Molecular beam mass-spectrometer (MBMS) sampling allows detection of

radicals and other unstable species but disturbs the flame more significantly and, therefore, has lower spatial resolution than the microprobe sampling technique.

To interpret the sampling measurements correctly, an analysis of the probe-induced perturbations is needed. The distortions caused by the probe can be divided into internal and external ones, the latter being gas dynamic and thermal. The probe acts as a sink for matter and heat and causes distortions of temperature and species concentration profiles. This results in distortions of lines of equal temperature and concentration in the flame flow field, which are planar one-dimensional in the absence of the probe.

The probe sampling factor α seems to be one of the important characteristics of gas dynamic interaction between the probe and the flame. It is defined as

$$\alpha = 4G/\pi d^2 \rho_0 w_0, \tag{1}$$

where G is the gas flow rate through the probe orifice with diameter d and ρ_0 and w_0 are the density and velocity of undisturbed flow at the burner surface.

The thermal interaction between the flame and the probe surface affects the chemical processes in the flame and the sample composition. Thus, they should be taken into account in interpreting the results obtained by probe sampling.

In the literature, there are many simplified theoretical approaches [1–7] to account for probe-induced perturbations of the flame structure, when interpreting the results obtained by probe sampling. However, an accurate solution of the problem is not available because of its complexity.

The velocity field and streamlines near the probe orifice were first calculated by Rosen [1] for a disk sink model. Various aspects of the probe effects in flames were considered in a series of papers by Hayhurst *et al.* [2–4], Dubinin *et al.* [5], and Smith [6]. Yi and Knuth [7] solved the gas dynamic problem of determining the distribution of flow parameters near the sink orifice of a conical probe under the assumption of inviscid flow and using a solution of the problem of a point sink in an incompressible fluid with corrections made for compressibility effects. The concentration evolution was treated as a self-diffusion process in a binary gas mixture. Comparing concentration profiles obtained with and without the probe, they established that these profiles can be characterised by the apparent shift δ given by the relation $\delta/d = 0.19(\mathrm{Re}\, Sc)^{1/2}$, where Re is the Reynolds number, determined by the gas parameters in the plane of the probe orifice and the orifice diameter d, and Sc is the Schmidt number. The gas streamline pattern near the probe tip has been demonstrated in a number of papers [3, 4, 8]. The main feature of the flow is the direction of the streamlines bounded by the stagnation line to the probe orifice.

Along with theoretical predictions, there has been a review [9] and many experimental studies of the problem discussed here. The influence of the external diameter of the "sonic" probe tip (0.5–2 mm) and the cone angle on the O_2 concentration profile in an atmospheric methane/oxygen flame was studied experimentally by Yoon and Knuth [10]. The effect of a "sonic" probe on the temperature field in a low-pressure flame was investigated by Hartlieb *et al.* using laser-induced-fluorescence of OH and NO [11]. In the vicinity of the nozzle tip, the decrease of temperature due to the nozzle cooling effect was observed. The thermal effect of a probe on a flame as a function of the cone angle of the probe was examined by Biordi *et al.* [12]. They measured temperature profiles in methane/oxygen/argon flames at $\sim$0.04 atm using Pt-Pt 10% Rh thermocouples directly in front of the probe tip at a distance equal to two orifice diameters. An average decrease of 200 K in gas temperature was observed for probes with cone angles of up to 64°. Moreover, a probe with a cone angle of 78° was found to disturb the flame structure significantly. Comparison of temperature profiles

with and without the probe in 40 torr CH_3 OH/air flame is shown in [13]. Struckmeier *et al.* [14] present a huge amount of experimental work on probe perturbations, with particular attention given to the effect of cooling the flame with the probe located at various positions from the burner surface. Earlier [15], it was shown that at sampling of flame by a microprobe, a shift of methane concentration profile with regard to the profile measured by optical method is observed.

The profiles of OH mole fraction measured by mass-spectrometry and absorption spectroscopy methods are presented in [16]. Probe effects in flame and heat transfer between the probe and the flame were studied by Emel'yanov *et al.* [17]. They considered a probe with geometry close to the real one and determined the coefficients of heat transfer between the probe and flame using experimental data. There are several methods for measuring temperature profiles in flames: thermocouple, spectroscopic, and two other methods in which the sampling probe is used as a temperature measuring device. These methods are the pneumatic probe technique [18], which was employed by Kaiser *et al.* [19] and Nogueira *et al.* [20], and the time-of-flight technique [10, 21]. In the pneumatic probe technique, the choked flow relation for the gas flow rate through the probe orifice is used.

In addition to the shift of concentration profiles and cooling of the gas entering the probe, a sample of a flame is changed during its passage through boundary layers (on the high pressure side of the sampling cone), i.e. on its way to the narrowest part of the sampling orifice [22]. Burdett and Hayhurst measured this "boundary layer cooling" and found how it depended on the diameter of the sampling hole. That study indicated that in sampling a flame, ideally one must always make measurements with orifices of different diameters. Such information reveals whether the perturbations are primarily in the boundary layers or in the supersonic expansion [23]. However, it seems that this problem cannot be solved by simply changing the orifice diameter. The effect of the probe walls should be taken into account when using a microprobe with a molecular flow, and in the case of "sonic" probe and MBMS, the effect of the boundary layer of the probe on the chemical composition of the sample is much weaker. Next, there are perturbations in the supersonic expansion inside the sampling cone, which have been studied in detail by Hayhurst and Telford [24]. In the present paper, however, we restrict ourselves to the processes that occur with a sample before it enters the orifice of the sampling cone. In a further model we plan to include the internal part of the probe tract in the simulation domain.

The correction of the thermal perturbation of the probe consists of measuring the "perturbed" temperature profile with a microthermocouple whose junction is placed at about two diameters of the probe orifice in front of the sampling tip [25–27] or perturbed temperature profiles were obtained using the choked probe technique [14, 20]. One of the main objectives of flame structure studies is to establish the mechanism of chemical reactions by comparing experimental and simulation results. An interesting approach to achieve this objective in spite of flame perturbations by the probe was used in [28]. In this work, experimental species concentration profiles were compared with those calculated with the PREMIX code using a detailed chemical kinetic mechanism and the "perturbed" temperature profile measured with a thermocouple positioned at a certain distance from the probe tip. A similar approach was employed in [29, 30], where perturbed temperature profiles were obtained using the choked probe technique.

In [31], the following approach was used to account for the influence of the probe on the flame. In comparing experimental and simulation results, which is necessary for the validation of the mechanism, one must take into account the thermal and gas-dynamic perturbations of the flame by the probe. Gas-dynamic perturbations were considered using

the semi-empirical relation

$$\delta = 0.37d\sqrt{\alpha} \tag{2}$$

obtained in [15]. Thermal perturbations were taken into account in the modelling by using the temperature profile obtained with a thermocouple placed in front of the probe, at a distance of 0.2 mm (or 2.5 d) from its end. When the results of the experiment and simulation were compared, the experimental profiles were shifted a distance δ upstream, allowing a correct comparison between the experiment and simulation. This procedure was also used in [32, 33]. In [33], δ was defined as $\delta = 0.2d\sqrt{\alpha}$.

The results of papers [28–33] reflect the close internal relationship between local temperature and mixture composition in the flame flow perturbed by the probe, although the range of applicability of these approaches is not completely clear.

Generally, the theoretical approaches used in the literature to evaluate the gas dynamic effects of the probe are highly simplified. As a rule, these approaches are based on approximating the flow field near the probe by incompressible fluid flow without due regard to the particular probe geometry. This study represents the first attempt to model the real interaction between a probe (of a specific shape and size used specifically in flame probing experiments) with a real flame (with a description of the basic parameters of the flame). The data demonstrating the nature of the probe-perturbed flame under conditions close to real ones were obtained for the first time.

2. Experimental

A premixed laminar $CH_4/O_2/Ar$ (lean, 0.06/0.15/0.79, equivalence ratio $\varphi = 0.8$) flame was stabilised at a flow rate of 25 cm^3/s on a Botha–Spalding burner 16 mm in diameter at a pressure of 1 atm (735–762 torr) and an unburned-gas temperature of about 368 K. The burner surface was a brass disc with holes 0.5 mm in diameter. The burner was moved along its axis to provide sampling by a fixed probe. The Pt-Pt 10% Rh thermocouple used in flame temperature measurements was made from welded 0.02 mm diameter wires and covered by a thin layer of SiO_2 to prevent catalytic recombination of radicals on the surface. Spatial profiles of CH_4 and H_2O were measured by MBMS. The molecular-beam setup based on an MS-7302 quadrupole mass-spectrometer was described in detail previously [34, 35]. The measurements were performed using a quartz sonic probe with a tip orifice diameter of 80 μm, an inner cone angle of 40°, an outer cone angle of 51°, and a tip diameter of 240 μm (wall thickness near the tip of 80 μm). The conical part of the probe from the tip to the base of the cone was 20 mm long. A skimmer with a 0.6 mm orifice was at a distance of 20 mm from the probe orifice. Figure 1 shows a scaled diagram of the burner surface, the probe at 0.8 mm from the burner, and the skimmer. Temperatures of the probe tip and the cone walls at various distances from the tip were measured by the thermocouple. The error of the thermocouple measurements was within ±30 K.

Figure 2 shows measured temperatures of the probe tip and two points on the cone wall as a function of the distance between the burner and the thermocouple position. The measurements were performed using a Pt-Pt 10% Rh thermocouple 20 μm in diameter coated with SiO_2. The thermocouple was attached to the probe at one of three points by the way of its tension, then the burner was moved relative to the probe. In this case, the distance between the tip of the probe and the surface of the burner varied in the range from 0.1 to 3.5 mm. For comparison, this figure also gives a temperature profile in the unperturbed flame, i.e. in the absence of the probe in the flame, calculated with the PREMIX code [36]

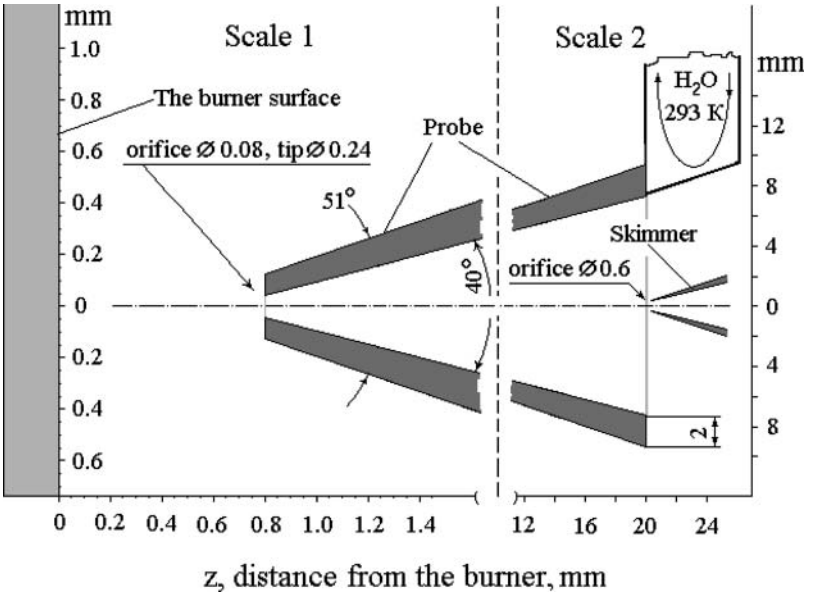

Figure 1. Diagrammatic representation of the surface of burner, probe, and skimmer, drawn on scales 1 and 2. The dimensions of the openings and tip of probe are given in millimetres.

from the Chemkin II package [37] using the GRI 3.0 mechanism for methane oxidation [38]. As can be seen from these data, the width of the flame front is about 1 mm, and the difference in temperature between the unperturbed flame and the probe wall reaches 350–600 K.

3. Gas dynamic structure of the flow

The flow between the burner and the axisymmetric probe in the flow was simulated using the full set of unsteady Navier-Stokes equations. For an approximate consideration of the heat release due to the chemical reactions, a source term Q_T is added to the energy equation to provide the given temperature distribution in the planar, undisturbed, isobaric flame, i.e. in the absence of the probe in the flame.

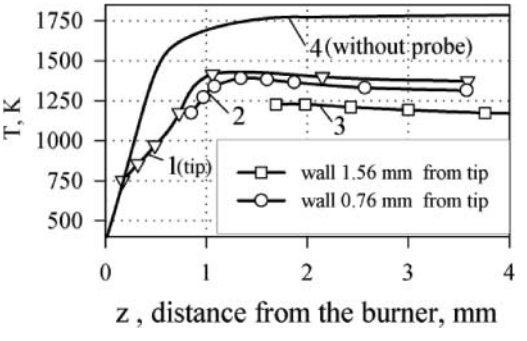

Figure 2. Temperatures measured at the probe tip (curve 1) and at two points on the cone wall (curves 2 and 3) as a function of the distance between the burner and the thermocouple position. The temperature profile in the unperturbed flame (in the absence of the probe in the flame, curve 4) is shown for comparison.

The main features of the recently developed original algorithm used to solve the Navier-Stokes equations are described below.

3.1 *The governing equations*

The governing system of equations for two-dimensional flow with plane ($\nu = 0$) or axial ($\nu = 1$, y and z are the radial and axial coordinates, respectively) types of symmetry have the usual form and include the continuity equation

$$\frac{D\rho}{Dt} + \rho \cdot \operatorname{div} \vec{\mathbf{v}} = 0, \tag{3}$$

the two momentum equations

$$\rho \frac{Du}{Dt} + \frac{\partial p}{\partial y} = \frac{\partial \tau_{yy}}{\partial y} + \nu \frac{\tau_{yy} - \tau_{\theta\theta}}{y} + \frac{\partial \tau_{yz}}{\partial z}, \tag{4}$$

$$\rho \frac{Dw}{Dt} + \frac{\partial p}{\partial z} = \frac{\partial \tau_{zy}}{\partial y} + \nu \frac{\tau_{zy}}{y} + \frac{\partial \tau_{zz}}{\partial z}, \tag{5}$$

and the energy equation

$$\rho \frac{De}{Dt} + p \cdot \operatorname{div} \vec{\mathbf{v}} = -\frac{\partial q_y}{\partial y} - \nu \frac{q_y}{y} - \frac{\partial q_z}{\partial z} + \Phi + Q_T, \tag{6}$$

where

$$\frac{D}{Dt} = \frac{\partial}{\partial t} + u\frac{\partial}{\partial y} + w\frac{\partial}{\partial z},$$

$$\operatorname{div} \vec{\mathbf{v}} = \frac{\partial u}{\partial y} + \nu \frac{u}{y} + \frac{\partial w}{\partial z},$$

$$\Phi = \tau_{yy}\frac{\partial u}{\partial y} + \nu \tau_{\theta\theta}\frac{u}{y} + \tau_{zz}\frac{\partial w}{\partial z} + \frac{\tau_{zy}^2}{\mu},$$

$$\tau_{yy} = 2\mu \frac{\partial u}{\partial y} + \left(\mu' - \frac{2}{3}\mu\right) \cdot \operatorname{div} \vec{\mathbf{v}},$$

$$\tau_{zz} = 2\mu \frac{\partial w}{\partial z} + \left(\mu' - \frac{2}{3}\mu\right) \cdot \operatorname{div} \vec{\mathbf{v}},$$

$$\tau_{\theta\theta} = 2\mu\nu \frac{u}{y} + \left(\mu' - \frac{2}{3}\mu\right) \cdot \operatorname{div} \vec{\mathbf{v}},$$

$$\tau_{yz} = \tau_{zy} = \mu \cdot \left(\frac{\partial u}{\partial z} + \frac{\partial w}{\partial y}\right),$$

$$q_y = -\lambda \frac{\partial T}{\partial y}, q_z = -\lambda \frac{\partial T}{\partial z}.$$

Here u and w are the radial and axial components of the total velocity, ρ is the density, p is the pressure, T is the temperature, e is the specific internal energy, μ is the dynamic viscosity, μ' is the bulk viscosity, and λ is the heat conductivity. The source term mentioned above, Q_T, in Equation (6) is described below in Section 3.4. To close the system of

Equations (3)–(6), the following relations are used assuming the gas to be perfect:

$$p = \rho \cdot R \cdot T.$$

$$e = \frac{1}{\kappa - 1} \cdot R \cdot T,$$

where R is the gas constant and κ is the specific heat ratio.

3.2 *Finite-difference scheme*

The main features of the finite-difference scheme used are as follows:

i) Finite-difference approximation of the governing equations is performed on a staggered grid, where pressure, density, temperature, and the transport coefficients are defined at the centre of the cell, while the velocity components are defined at the middle of the corresponding boundaries of the cell.
ii) The finite-difference equations are solved implicitly using the well-known method of splitting into physical processes and spatial variables [39]. At each fractional step, the standard tridiagonal matrix algorithm is applied.
iii) The continuity equation is approximated according to the scheme providing conservation of variables, when a steady solution is obtained (or when the equations are resolved explicitly).
iv) The centred approximation of difference operators provides second-order accuracy over the spatial variables on the uniform grid.
v) The algorithm is characterised by low implicit artificial viscosity, which significantly extends the range of Reynolds numbers available for modelling.

The staggered grid was proposed before [40] and is widely used for simulating incompressible flows. Our experience shows, however, that this grid is also preferred for simulating highly compressible flows [41, 42].

3.3 *Simulation domain and boundary conditions*

The existing version of the algorithm operates with a uniform rectangular grid with mesh sizes *dy* and *dz* in radial and axial directions, respectively. The simulation domain consists of a number of straight lines parallel or perpendicular to the axis and one line with arbitrary inclination to the axis. The cells in the vicinity of this line have a triangular or trapezoidal shape; this necessitates some modification of the finite-difference relations used here to provide second-order accuracy of the scheme.

A diagram of the simulation domain for a distance between the probe tip and the burner $z_0 = 0.8$ mm is presented in Figure 3. The solid boundaries are shown by solid lines, and the permeable inlet and outlet boundaries by dotted lines. This domain corresponds to the shape of the sampling probe used in our experiments. The distance from the burner to the probe, z_0, was varied from 0.2 to 0.8 mm, and the axial length of the conical part of the probe was always 2 mm while the radial size of the domain was 1.5 mm. At the burner surface (line 1–7) the conditions for all the variables were defined based on the solution for the unperturbed isobaric flame obtained by the PREMIX code for the mixture considered (temperature $T = 368$K, axial velocity $w = 15.68$ cm/s, radial velocity $u = 0$). At the solid boundaries (lines 3–4–5–6), the normal velocity component was set equal to

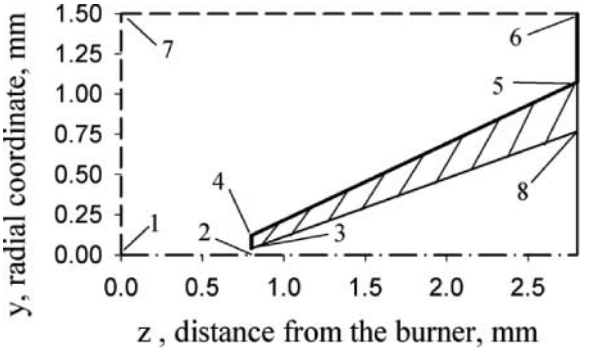

Figure 3. Diagram of the simulation domain. The distance between points 2 and 3 is the radius of the probe orifice, 3–4 tip of the probe, 4–5 external generatrix of the cone wall, 3–8 internal generatrix of the cone wall, z-axis – centreline of the probe through the centre of the probe orifice, y-axis – surface of the burner. Note that the internal part of the probe tract is not included in the simulation domain (see text).

zero, and the tangential component and the temperature were specified taking into account the velocity slip and temperature jump [42], although under the conditions used, the slip effects are insignificant. The temperature distribution over the probe surface was set based on thermocouple measurements. Figure 2 illustrates the results of these measurements for three points on the probe's surface, which were used for linear interpolation and extrapolation of temperature along the conical probe. There is no need to prescribe the pressure p or the density ρ at the solid boundaries. The conditions at the probe's orifice (lines 2–3, Figure 3) were obtained by extrapolation from internal points of the domain for all variables, except for the axial velocity, which was assumed to be equal to the local sound velocity. This assumption allows one not to consider the internal flow inside the probe, although it may lead to some inaccuracy in the flow description (the estimated discharge coefficient of the gas flow rate through the probe is about 0.9 and not 1 as is assumed). At the upper permeable boundary (line 7–6), an attempt was made to specify all the variables by extrapolation from the interior. The simulations show, however, that to obtain a stable solution for the highly subsonic flow considered, it is necessary to specify the pressure at this boundary [42]. The latter condition is equivalent to the presence of mass sources or sinks here. On the axis of symmetry (line 1–2), the radial velocity and the radial derivatives of the axial velocity and temperature were set equal to zero.

The mesh size dy in the radial direction was 2.5 μm; thus, the number of cells was 16 over the radius of the probe orifice, 48 over the radius of the probe tip and 600 over the radius of the domain. The mesh size dz in the axial direction was slightly different from dy and was about 2.62 μm. This value is due to the ratio between dy and dz in the case considered, where the simulation domain contains a line with an arbitrary inclination to the axis (see Figure 3) [41, 42].

3.4 *The source term for the energy equation*

The simulations were performed for the burner-stabilised premixed flame studied in the experiments. The combustible gas mixture was assumed to be a single-component perfect gas with a molecular weight of 37.32 kg/kmol and a specific heat ratio $\kappa = 1.5747$ calculated from the real parameters of the flame at the burner surface. The temperature dependence

of the dynamic viscosity μ of the gas was described by the Lennard-Jones (6–12) potential with parameters $\sigma = 3.418$ Å and $\varepsilon/k = 124$ K typical of argon [43]. Since the main component of the mixture is argon, the value of the Prandtl number ($\mathrm{Pr} = \mu C_p/\lambda$) was assumed to be the same as for a monatomic gas, i.e., $\mathrm{Pr} = 2/3$. The effect of bulk viscosity was neglected ($\mu' = 0$).

For the numerical solution, the variables ρ, p, T, u, and w were normalised by the corresponding parameters at the burner surface (below denoted by the subscript $_0$), including the speed of sound $c_0 = 359.3$ m/s. The spatial variables y and z were conveniently expressed in mm.

As was mentioned above, to approximately account for the heat release due to chemical reactions, we added a source term, Q_T, to the energy equation. To identify the main features of sampling, it proved necessary to assume a two-dimensional problem could be treated by assuming a source term only depends on z. This approach can be amended later. Thus $Q_T(z)$ provides the given temperature distribution in the undisturbed isobaric flame, i.e. in the absence of the probe in the flame. This term was obtained from the following relation representing the condition for steady solution of energy equation, Equation (6), written in non-dimensional form:

$$\frac{\partial \tilde{T}}{\partial \tilde{t}} = \tilde{Q}_{T,conv} + \tilde{Q}_{T,vis} + \tilde{Q}_T = 0, \tag{7}$$

where the convective terms in the energy equation, Equation (6), are schematically denoted by $\tilde{Q}_{T,conv}$, the viscous terms are denoted by $\tilde{Q}_{T,vis}$, and the $\sim$ over a symbol is used to denote dimensionless variables. The finite-difference representation of relation (7) for one-dimensional flow was performed on the same staggered grid for the axial coordinate as in two-dimensional calculations below, with the source term being defined at the centre of the cell. The temperature distribution in the flow was set in accordance with the results of simulating the undisturbed flame flow with the Chemkin PREMIX code [36]. This distribution is shown in Figure 2. The distributions of the density and axial velocity in relation (7) were found from the continuity equation, Equation (3), and the equation of state, assuming the pressure to be constant and equal to 760 torr. For the source term to be consistent with the flow model considered, we neglected small changes in the mean molecular weight, occurring in the real undisturbed flame due to chemical reactions.

The obtained axial dependence of $\tilde{Q}_T(z)$ is illustrated in Figure 4. Positive values reflect heating by exothermic chemical reactions, occurring in the oxidation of CH_4, as discussed below. The visible oscillations, which have a negligibly small effect on the results, are due to some inaccuracy in the approximation of the temperature distribution. To convert the shown non-dimensional source term $\tilde{Q}_T(z)$ to the term $Q_T(z)$ entering the right side of the energy equation, Equation (6), in dimensional form (in units of power/volume), the values shown in Figure 4 should be multiplied by $(e_0 c_0 \rho(z)/h_0)$, where $h_0 = 1$ mm is the unit used for linear variables, and $\rho(z)$ is the dimensional density in the undisturbed flame. Thus, at $z = 0.523$ mm, where the source term $\tilde{Q}_T$ reaches its maximum non-dimensional value of 0.03676 (see Figure 4), the corresponding dimensional value is $Q_T = 0.0159$ W/m^3. The small values of $\tilde{Q}_T$ at $z \leq 0.2$ mm reflect the predominant effect of thermal conduction on the temperature profile in this region of the flame front. In a two-dimensional test simulation of the flow with the source term in the case of no probe present in the flow field, purely planar one-dimensional flow was obtained with a good representation of the temperature distribution in the undisturbed flame. It is assumed, therefore, that the flow field conditions near the probe are similar to those in the real flame.

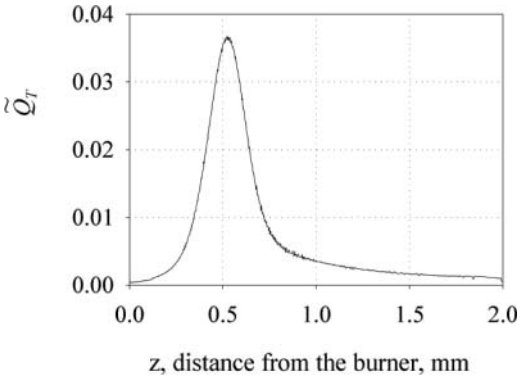

Figure 4. Source term in non-dimensional form for the energy equation obtained from relation (7) for a flame of methane. For the conversion of the source term on the right side of the energy equation, Equation (6), to dimensional form (in power/volume), see the text.

3.5 *Numerical procedure and test simulations*

The simulations were performed for four burner-to-probe distances (z_0): 0.2, 0.4, 0.6, and 0.8 mm. The initial distribution of the parameters in the simulation domain was assumed to be the same as in the undisturbed flame. In the presence of the probe, this distribution is violated due to the presence of solid surfaces in the flow field, the suction of gas at the probe's inlet, and heat transfer between the gas and the probe. As a result, the flow begins to change, and after some time, it reaches a steady state.

The sizes of the computational domain indicated above and the mesh sizes *dz* and *dr* were chosen after a series of test calculations and seem to be close to optimal. Thus, when the mesh sizes *dz* and *dr* were increased by a factor of two (compared to the base case) and, accordingly, 8 cells fell on the radius of the probe orifice, there was a significant, ∼10% increase in the gas flow rate through the probe, due to increasing density near the edge of the orifice because of the insufficiently accurate description of the flow field characterised by the presence of large gradients of the parameters in this region of the flow. On the flow axis, which is of particular interest from the standpoint of comparison with experiment, the difference in flow parameters was much smaller and did not exceed 2%. When the mesh sizes *dz* and *dr* were decreased by a factor of 1.5 and 24 cells fell on the radius of the probe orifice, a small, ∼ 2% reduction in the gas flow rate through the probe was observed and the change of the parameters on the flow axis did not exceed 1%. Therefore, we may conclude that the obtained numerical solution of the finite-difference equations provides quite an appropriate solution to the initial differential equations.

The results of some test calculations of the gas flows made by the developed algorithm have been reported earlier [41, 42]. In paper [44] the developed model was used for numerical simulation of thermocouple-induced perturbations of the methane flame structure.

4. Results

Figure 5 illustrates the streamline pattern for $z_0 = 0.8$ mm. The flow rates indicated in the figure are expressed as the sampling factor α (see Equation (1)), where G is the flow rate between the given streamline and the centreline. It is evident that the probe produces strong disturbances of the flame's flow field. At some distance from the probe tip (∼0.52 mm), a stagnation point is formed on the surface of the probe cone, which is typical of the flow

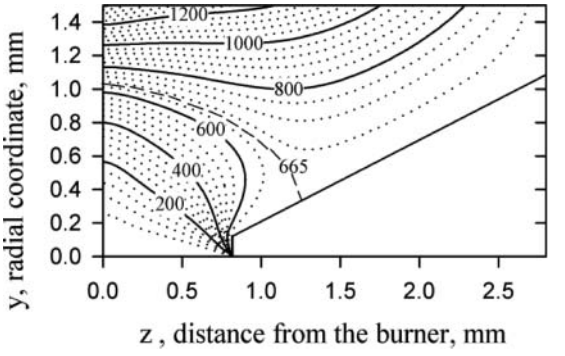

Figure 5. Streamline pattern for $z_0 = 0.8$ mm. Numbers on the line correspond to the values of the sampling factor α. The stagnation line abuts the probe wall at 0.52 mm from its tip.

considered [2, 6, 7]. In this case, part of the gas flowing through the orifice comes from the boundary layer. It is estimated that for the relative position of the skimmer and probe orifice used in the study, the gas flow rate entering the skimmer reaches ∼1/600 of the gas flow rate through the probe. The radius of the corresponding streamtube in the plane of the probe orifice is ∼1.6 μm, which excludes any significant influence of the boundary-layer gas entering the probe on this axial flow region.

The field of isotherms for $z_0 = 0.8$ mm is illustrated in Figure 6, which also shows strong disturbances of the flame flow field. The cooling effect at the flow's periphery by the cone is quite pronounced. In the near centreline region, a marked downstream shift of the isotherms takes place.

The axial distribution of the flow parameters for $z_0 = 0.8$ mm is illustrated in Figure 7. The temperature distribution in the unperturbed flow is given for comparison. The axial velocity (w) increases monotonically from the value at the burner's surface to the sonic value at the inlet orifice. The pressure (p) remains almost constant over most of the distance to the probe tip, except in the vicinity of the tip (∼0.05 mm), where the pressure decreases by a factor of about two due to suction by the probe. As a result of this pressure behaviour, the temperature and density profiles are almost inverse to each other (n is the number density). The increase in the temperature (T) with increasing z is significantly lower than

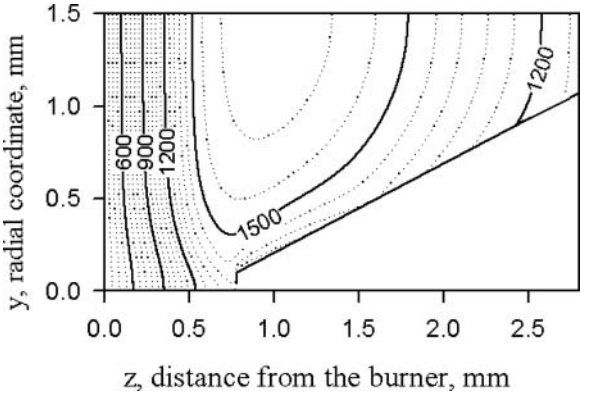

Figure 6. Field of isotherms for $z_0 = 0.8$ mm. Temperature is in degrees K.

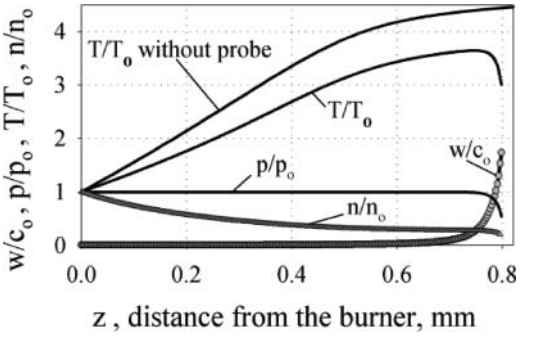

Figure 7. Axial distribution of parameters for $z_0 = 0.8$ mm. The temperature (T), pressure (p), and number density (n) are normalised by the corresponding parameters on the burner surface (T_0, p_0, n_0), and the axial velocity (w) is normalised to the speed of sound in the gas on the burner surface (c_0).

that in the unperturbed flame, in spite of the effect of the source term. This is due to the flow accelerating, which considerably reduces the residence time of the gas in the region of a heat source of given intensity. In the vicinity of the probe's orifice, the temperature even decreases due to rapid acceleration of the transonic flow. The axial distributions of the parameters for the other distances z_0 are similar to those discussed above.

The radial distribution of the parameters at $z_0 = 0.8$ mm in the plane of the orifice is illustrated in Figure 8. The results are shown for the meshes nearest to the tip. For the axial velocity, these points correspond exactly to the plane of the tip, and the other quantities are shown at a distance $dz/2$ from the plane of the tip.

In the range of radii corresponding to the position of the orifice ($y \leq 0.04$ mm), the radial velocity is negative, which reflects suction by the probe. In the vicinity of the orifice edge, both the axial and radial velocities are close to the speed of sound. The temperature increases with radius due to the weakening of the suction by the probe. In the range 0.04 mm $< y < 0.12$ mm, corresponding to the surface of the probe's tip, the gas temperature is almost constant and equal to the surface temperature, while for $y > 0.12$ mm, there is a slight increase in the temperature to its value in the undisturbed flow. For $y \leq 0.04$ mm, the axial velocity is exactly sonic due to the boundary conditions used, and hence it reflects the

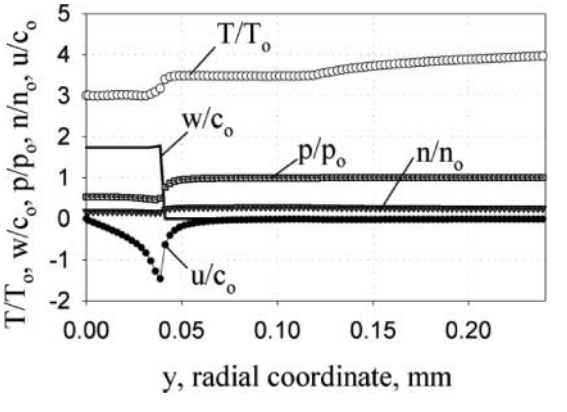

Figure 8. Radial distribution of flow parameters in the plane of the probe tip for $z_0 = 0.8$ mm.

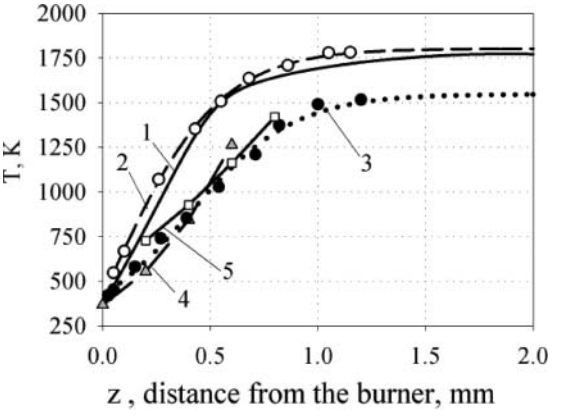

Figure 9. Temperature profiles in the methane flame without the probe and in the presence of the probe on its axis: 1 and 2 – without the probe, 1 – calculation using PREMIX (solid line), 2 – thermocouple measurements (○ – measurements, dotted line – smoothed curved through the measured points), 3 and 4 – temperature at 0.2 mm from the probe tip (3 – profile measured by the thermocouple, • – measurements, dotted line – smoothed curve, 4 – profile calculated by the model, triangles – calculated points, dashed line – smoothed curve), 5 – profile calculated by the choked probe technique (squares – calculated points, solid line – smoothed curve).

behaviour of the temperature. In the range 0.04 mm $< y <$ 0.12 mm, the axial velocity is zero, and for $y >$ 0.12 mm, it has small negative values due to inverse flow here (see Figure 5). The pressure is almost constant for all radii except in the range $y \leq$ 0.04 mm, where it decreases by about a factor of 2. Due to the equation of state, the radial dependence of density is a consequence of the dependencies on temperature and pressure. The radial distributions of the parameters for the other distances, z_0, are similar to those discussed above.

Figure 9 shows temperature profiles obtained numerically and experimentally. The unperturbed profile (1) was calculated using the PREMIX code (the same as shown in Figure 2), and the profile (2) was measured using a thermocouple without a sampling probe in the flow (smoothed temperature profiles obtained by the thermocouples with a radiation correction applied). The correction for heat losses due to radiation was calculated by the formula proposed [45] for a circular thermocouple, with an equivalent diameter of the ribbon thermocouple determined as the ratio of the thermocouple cross-sectional perimeter to π [46]. The temperature dependence of the emissivity ε_T of the thermocouple coated with SiO_2 was taken into account. For fused quartz, this dependence [47] can be approximated by the formula

$$\varepsilon_T(T) = 0.163297 + 0.766332/(1 + \exp((T - 583.467752)/146.53391))^{0.317496}$$

where the temperature T is in Kelvin. This relation was determined by approximating the measurements obtained in the temperature range of 300 to 1700 K.

The calculated and measured data are in satisfactory agreement, although there is a noticeable difference between them. The profile (3) was measured by a thermocouple directly in front of the probe at a distance of 0.2 mm from the tip; the profile (4) represents the calculated temperature on the flow's centreline, with the probe orifice located at the distances, z_0. One can see that both the calculated and measured perturbed profiles are

0.2–0.3 mm downstream of the unperturbed temperature distribution. The calculated and measured profiles are quite similar, suggesting that the model adequately describes the main features of the flow. The profile (5) represents the temperature obtained from calculated values of α by isentropic relations for critical flow through a de Laval nozzle. These data can be treated as the temperature "measured" by the choked probe. This profile is also in good agreement with the thermocouple measurements, indicating some similarity between the approaches used previously [14, 20, 29, 30] and [25–28, 31–33] to take into account the effect of probe-induced flame perturbations on concentrations of various species.

5. Distribution of concentrations

The obtained gas dynamic structure of the flow near the probe under conditions similar to those in a real perturbed flame was used to evaluate the probe-induced perturbations of species concentrations – the most important problem from an experimental point of view. Since the main component of the investigated flame is chemically neutral argon, the evolution of the concentration of some flame species in the flow field was simulated using the diffusion equation:

$$\rho\frac{\partial c_1}{\partial t}+\rho u\frac{\partial c_1}{\partial y}+\rho w\frac{\partial c_1}{\partial z}=-\frac{1}{y^\nu}\frac{\partial}{\partial y}\left(y^\nu J_{1y}\right)-\frac{\partial}{\partial z}J_{1z}+Q_c, \tag{8}$$

for binary gas mixtures of these species with argon (species 2) for plane ($\nu = 0$) or axisymmetric ($\nu = 1$) flow. Here c_1 is the mass fraction of species 1 and Equation (8) is only for a non-reacting mixture. The effect of chemical reactions was approximately described by a source term, Q_c, which provided a given species concentration distribution in the unperturbed flame, i.e. in the absence of the probe in the flame. The diffusion fluxes, J_{1y} and J_{1z}, include the concentration, pressure, and thermal diffusion terms and are expressed as

$$J_{1y}=-\rho D_{12}\left[\frac{\partial c_1}{\partial y}+\frac{m_2-m_1}{m}c_1(1-c_1)\frac{\partial \ln p}{\partial y}+\frac{m_1m_2}{m^2}k_T\frac{\partial \ln T}{\partial y}\right],$$

$$J_{1z}=-\rho D_{12}\left[\frac{\partial c_1}{\partial z}+\frac{m_2-m_1}{m}c_1(1-c_1)\frac{\partial \ln p}{\partial z}+\frac{m_1m_2}{m^2}k_T\frac{\partial \ln T}{\partial z}\right],$$

where D_{12} is the binary diffusion coefficient, m_1 and m_2 are the molecular weights of species 1 and 2, m is the mean molecular weight, and k_T is the thermal diffusion ratio.

The diffusion equation was solved using the same staggered grid and finite-difference scheme as in the gas dynamic simulation, with the concentration being determined at the centre of the cell. The problem was treated in a linear formulation, i.e., neglecting the effect of diffusion on the flow field parameters. Four flame species were considered: CH_4, CO_2, H_2O, and O_2, although this approach can be used to analyse the evolution of concentrations of any flame species. The source term, Q_c, depended only on z and was obtained in the same way as the source term for the energy equation described above, i.e. from the following relation representing the condition for steady solution of the diffusion equation, Equation (8), written in non-dimensional form:

$$\frac{\partial c_1}{\partial \tilde{t}}=\tilde{Q}_{c,conv}+\tilde{Q}_{c,diff}+\tilde{Q}_c=0, \tag{9}$$

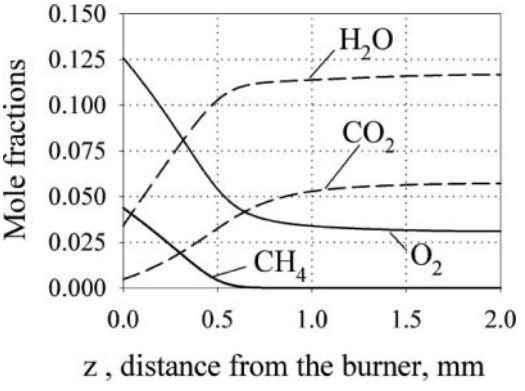

Figure 10. Distributions of species concentrations in undisturbed flame.

where the convective contribution to the rate in the diffusion equation, Equation (8), is denoted by $\tilde{Q}_{c,conv}$ and the diffusion rate – by $\tilde{Q}_{c,diff}$. Finite-difference representation of relation (9) for one-dimensional flow was performed on the same staggered grid for the axial coordinate as in the two-dimensional calculations, with the values of the source term being defined at the centre of the cell. The distributions of temperature, density, and axial velocity in the flow were specified in the same manner as in Section 3.4 during the calculations of the source term for the energy equation. The distribution of molar concentrations of the species considered was set in accordance with the results of simulation of the undisturbed flame flow by PREMIX code [36]. These distributions are illustrated in Figure 10 (it should be noted that within the framework of the approach used here, all other components of the flame are replaced by argon molecules).

The temperature dependence of the diffusion coefficients ρD_{12} for the investigated mixtures was described by the Lennard-Jones (6–12) potential [43] with parameters $\sigma = 3.746$ Å, $\varepsilon/k = 141.4$ K for CH_4, $\sigma = 3.763$ Å, $\varepsilon/k = 244$ K for CO_2, $\sigma = 2.605$ Å, and $\varepsilon/k = 572.4$ K for H_2O and $\sigma = 3.458$ Å, and $\varepsilon/k = 107.4$ K for O_2 using the conventional combination rules for describing the interaction between unlike molecules [43]. The contributions of pressure and thermal diffusion to the concentration distribution in the flow field were found to be small. The results presented below were thus obtained taking into account only concentration diffusion.

The obtained axial dependencies of $\tilde{Q}_c(z)$ for the species considered are shown in Figure 11; positive values are observed for the combustion products CO_2 and H_2O, and negative values for the reagents CH_4 and O_2. To obtain the source term on the right side of the diffusion equation, Equation (8), in units of mass per unit time per unit volume, the values shown in Figure 11 should be multiplied by $(c_0\rho(z)/h_0)$, where $h_0 = 1$ mm is the unit used for linear variables and $\rho(z)$ is the dimensional density in the undisturbed flame. The small values of $\tilde{Q}_c$ at $z \leq 0.2$ mm are indicative of the predominantly diffusive nature of this region of the flame front.

The boundary conditions for the diffusion equation were specified as follows. At the burner surface (line 1–7, see Figure 3), the concentration was set equal to that in the unperturbed flame. At the solid boundaries (lines 3–4–5), no diffusional flux was assumed since the consideration is limited to stable components of the flame that do not react with the surface of the probe. If the model is extended to radicals such as H and OH, the boundary conditions must be revised to account for the possible quenching of radicals on the surface

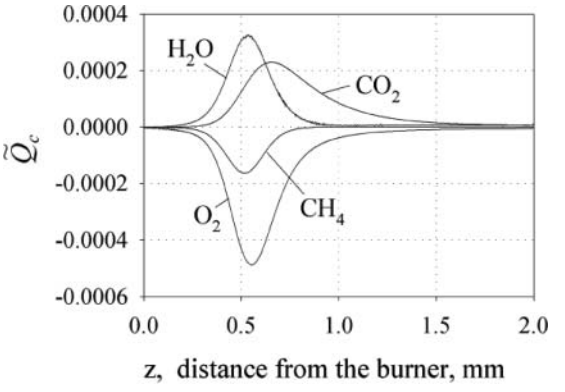

Figure 11. Source terms in non-dimensional form for the diffusion equation obtained from relation (9) for the flame components considered. For the conversion of the source term on the right side of the diffusion equation, Equation (8), to dimensional form (in mass/(time · volume)) see the text.

of the probe. In a simple formulation by introducing the probability of radical loss upon collision with the probe surface, we modelled the perturbations of H and OH radicals and the corresponding results will be published in a special paper.

On the probe near the orifice (line 2–3) and at the upper permeable boundary (line 7–6), the concentration was specified by extrapolation from the interior. On the axis of symmetry (line 1–2), the radial derivative of the concentration was set equal to zero. Finally, at the solid boundary (line 5–6), the concentration was assumed to be equal to that behind the unperturbed flame front.

Figure 12 shows axial distributions of the mole fraction of methane. For all values of z_0, the decrease in CH_4 with z is significantly less than that in the unperturbed flame, in spite of the effect of the source term, which is negative (see Figure 11). This is caused by the flow accelerating, which considerably reduces the residence time of the gas in the region, where $\tilde{Q}_c$ has a particular value. The concentrations at the centre of the inlet orifice are of greatest interest from an experimental point of view; they are shifted downstream of the position

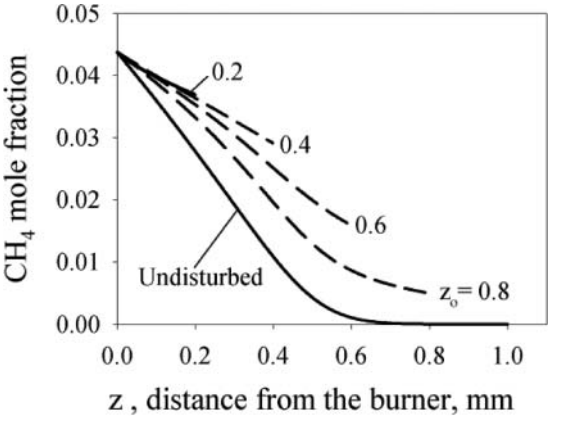

Figure 12. Axial distributions of methane mole fraction in the perturbed flow (dashed lines) for various positions of the probe in the flame. The unperturbed profile is also shown for comparison.

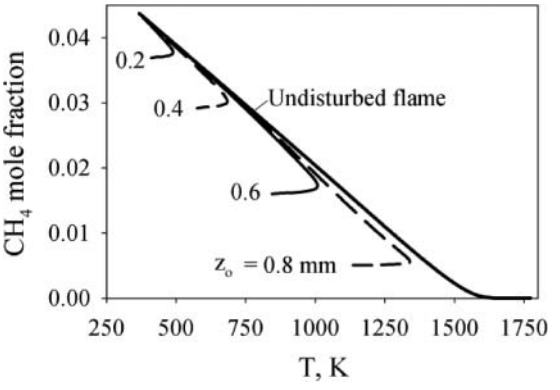

Figure 13. Similarity between the methane mole fraction and the temperature on the centreline of the perturbed flow for different positions of the probe in the flame.

of the same concentrations in the unperturbed flame. A comparison of these distributions with the axial temperature distribution (see Figure 7) shows their qualitative similarity, reflecting the well-known similarity between heat- and mass-transfer. The degree of this similarity is illustrated in Figure 13, where the mole fraction of methane on the axis of symmetry is plotted against the local temperature for the four cases considered. An analysis of these data reveals an important feature of the flame perturbed by the sampling probe: the relation between local concentrations and temperatures on the centreline of perturbed flame is close to that in the unperturbed flame. This rule is violated only in the close vicinity of the orifice, in which there is a rapid decrease in temperature due to huge acceleration of transonic flow (see Figure 7). These results allow one to explain the good agreement between the measured and calculated concentrations obtained before [28–33]. The axial concentration distributions for the other species considered have the same features as shown in Figures 12 and 13.

The undisturbed flame is planar and one-dimensional; therefore, no transverse gradients of parameters should affect the concentration distribution. As was mentioned above, the flow near the probe's tip is characterised by strong radial gradients of parameters (see Figure 8). In this respect, it is interesting to clarify the effect of the radial diffusional flux on the concentration distribution flow field. It is impossible to solve this problem experimentally, but it can be solved numerically neglecting the quantity J_{1y} in Equation (8).

Figure 14 illustrates the axial distributions of the mole fraction of CO_2 for $z_0 =$ 0.8 mm, as obtained with and without accounting for the radial diffusion flux. The significant effect of J_{1y} on the axial concentration distribution is evident – the CO_2 concentration is almost constant in the model with $J_{1y} = 0$ (curve 3) that differs significantly from the undisturbed profile (curve 1) which reveals the concentration rise due to chemical reactions. The curve 2 obtained with accounting for both components of diffusion fluxes lies much higher than the curve 3, though this curve is still lower than undisturbed one. A similar conclusion concerning the significant effect of J_{1y} on the axial concentration distribution can be derived from the radial concentration distributions in the plane of the inlet shown in Figure 15 for the same regime as in Figure 14. The highly non-uniform transverse distribution of concentration, caused by the different evolution of the parameters along the streamlines for $J_{1y} = 0$ is significantly smoothed if the radial diffusion is taken into account.

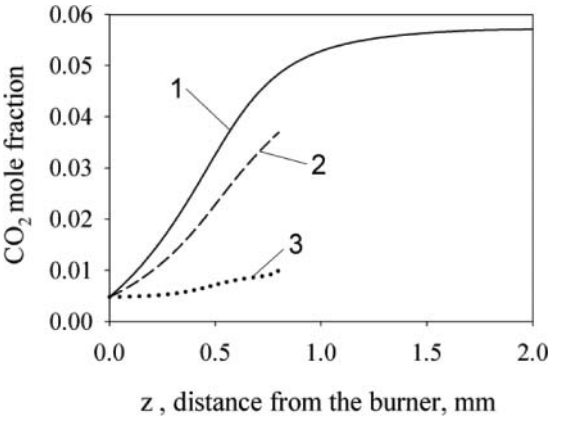

Figure 14. Effect of radial diffusion on the axial concentration profile of CO_2 for $z_0 = 0.8$ mm (1 – unperturbed profile, 2 – with this effect taken into account, 3 – neglecting this effect).

In view of the conservative nature of the pressure in the axial distribution of parameters illustrated above (see Figure 8), at the beginning of this study, we hoped to simulate the mixture's composition on the axis of the real flame using the PREMIX code [36] (operating with isobaric conditions) by specifying the streamtube's area on the flow axis. In this case, it would have been possible to calculate the perturbed concentrations in the vicinity of the probe's tip in the exact quasi-one-dimensional formulation. However, because of the strong effect of radial diffusion considered above, the idea makes no sense.

As can be seen from Figure 8, the difference between the perturbed and unperturbed concentrations at the same distance from the burner have a different sign at the centreline and at the periphery of the flow. This feature of the radial concentration distribution in the plane of the inlet was observed for all the regimes considered. It is due to the different evolution of the parameters along different streamlines and the reverse flow along the cone's surface near the tip of the probe (see Figure 5), resulting in sampling of the gas both

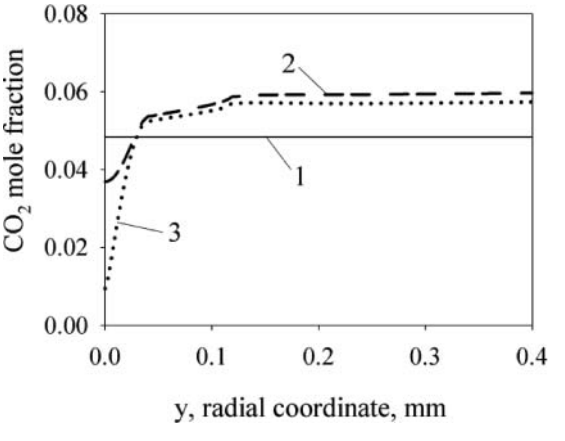

Figure 15. Effect of radial diffusion on the radial concentration profile of CO_2 in the plane of the probe tip for $z_0 = 0.8$ mm (1 – unperturbed profile, 2 – with this effect taken into account, 3 – neglecting this effect).

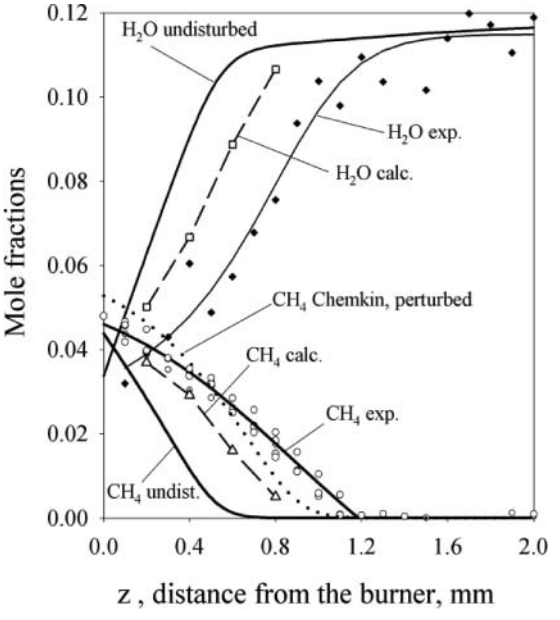

Figure 16. Various axial profiles of CH_4 and H_2O concentrations. For H_2O, three profiles are presented: the profile calculated for the undisturbed flame (H_2O undisturbed), the profile calculated using the model for four positions of the probe (H_2O calc.), and probe measurements (H_2O exp.) (filled points and smoothed curve). For methane, four profiles are presented: the profile calculated for the undisturbed flame (CH_4 undist.); the profile calculated using the model for four positions of the probe (CH_4 calc.); probe measurements (CH_4 exp.) (shown by circles and the solid line is smoothed curve); and the profile calculated by the PREMIX code from a temperature profile measured by the thermocouple in front of the probe tip at 0.2 mm from the tip (CH_4 Chemkin, perturbed) (dotted curve).

downstream and upstream of the probe [20]. A similar relationship between disturbed and undisturbed concentrations was found before [7], where the evolution of concentration was treated as self-diffusion in a simpler gas dynamic model of the flow.

A comparison of the calculated and measured concentration profiles of CH_4 and H_2O is presented in Figure 16, where the calculations correspond to the concentrations at the centre of the orifice. As can be seen from Figure 16, both the measured and calculated profiles are shifted downstream relative to the unperturbed ones, with the shift for the experimental profiles being about twice that for the calculated ones (the shift is the difference between the axial coordinates corresponding to the same concentration in the perturbed and unperturbed flames). Figure 16 also shows the profile of CH_4 (denoted as "CH_4 Chemkin, perturbed") calculated with the PREMIX code based on a temperature profile measured by a thermocouple in front of the probe (curve 3 in Figure 9), i.e., following the approach used before [28, 31–33]. These data are in a good agreement with the measurement results.

The values of the shift (δ) are summarised in Figure 17. The predictions of the approximate model [7] are also given for comparison. The dashed line ($\delta = z_0$) shows the maximum possible shift for a given distance, z_0. The systematic underestimation noted earlier of calculated data may be attributed to the non-linear effect of flow perturbations on the kinetics of chemical reactions. This effect cannot be taken into account in the developed model with spatially fixed sources of energy and concentrations.

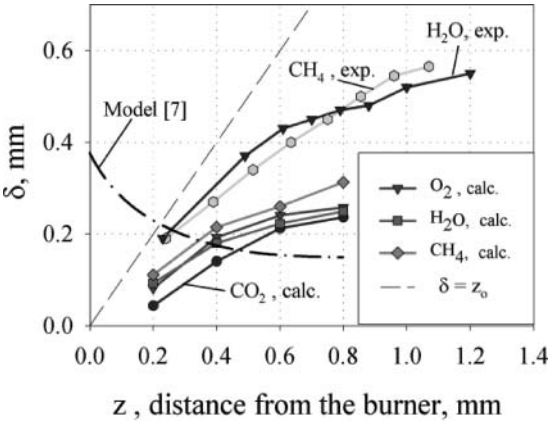

Figure 17. Shift (δ) of species concentration profiles relative to unperturbed ones. The shifts obtained from probe measurements of profiles are denoted by (exp.), those calculated for the model – by (calc.), and the shift denoted as model [7] is the shift calculated by the formula of Yi and Knuth [7]. The dotted line ($\delta = z_0$) corresponds to the maximum possible shift for the given distance from the probe to the burner surface.

The approximate relation for the shift available in the literature [7] can be used only for rough estimates. This relation predicts a decrease in the shift with increasing z_0, which is opposite to the results of measurements. Moreover, at small distances z_0, the corresponding predictions ($\delta > z_0$) have no physical meaning.

6. Conclusions

The main results can be summarised as follows:

1. A numerical model for the flow near the sampling probe, taking into account the effects of chemical reactions, was developed using the Navier–Stokes equations, completed by source terms for the energy and diffusion equations.
2. The model developed for the perturbed flame predicts a downstream shift of the main flow characteristics (temperature on the flow centreline, gas flow rate through the orifice, concentrations at the centre of the probe) relative to the characteristics of the unperturbed flame.
3. Temperature profiles in the unperturbed and perturbed flames were measured using a thermocouple. Measured temperatures in the perturbed flow are in satisfactory agreement with the calculated temperature on the flow centreline at the thermocouple's location (0.2 mm upstream of the tip), indicating that the model adequately describes the main features of the flow studied.
4. Concentration profiles of the main stable species in the flame were measured using the MBMS technique. The absolute value shift for these profiles (relative to the unperturbed profiles) increases with increasing distance between the probe and the burner; this is in agreement with the modelling, although the measured shifts are about twice the calculated values. The underestimation of shifts by the model may be attributed to the non-linear effect of flow perturbations on the kinetics of chemical reactions, which cannot be described in the model with spatially fixed sources of energy and concentrations.

5. The concentration profile for CH_4 calculated by the PREMIX code, based on the temperature profile measured by a thermocouple in front of the probe, i.e., following the approach used previously [28, 31–33], is in fairly good agreement with the MBMS data. However, the range of applicability of this approach needs further research.
6. The temperature deduced from the calculated values of the gas flow rate through the probe by the relation for the choked probe is in good agreement with the results of thermocouple measurements, indicating some similarity between the approaches used before [14, 20, 29, 30] and [28, 31–33] to take into account the effect of probe-induced perturbations on concentration profiles.
7. The relation between local concentrations and temperatures along the centreline of the perturbed flame is close to that in the unperturbed flame. This explains the good agreement between measured and calculated concentrations in the widely used approach to validating detailed reaction mechanisms, in which measured temperature profiles in perturbed flames were used for modelling [28–33].
8. The known feature of the transverse concentration distribution in the plane of the probe [7], where the difference between the perturbed and unperturbed concentrations at the same distance from the burner has different signs at the centreline and at the periphery of the flow is well reproduced by the model.
9. The simulations have revealed a significant effect of radial diffusion on the distribution of concentrations in the plane of the orifice. The effect of pressure- and thermal diffusion on the concentration distribution is relatively small.
10. The approximate relation for the shift available in the literature [7] can be used only for rough estimates.

In the further development of the flow model, instead of introducing spatially fixed source terms into energy and diffusion equations we are planning to use a simple model for chemical kinetics such as Zel'dovich's model or a Global Kinetics approach. This will provide a description of the non-linear effect of gas dynamic perturbations on chemical kinetics, which appears to be the main reason for the observed disagreement between the modelling predictions and experimental results.

References

[1] P. Rosen, *Potential flow of a fluid into a sampling probe*, Rept. CF-2248, Appl. Phys. Lab., Johns Hopkins Univ., Silver Spring, Md, 1954.
[2] A.N. Hayhurst and N.R. Telford, *Mass spectrometric sampling of ions from atmospheric pressure flames-I: Characteristics and calibration of the sampling system*, Combust. Flame 28 (1977), pp. 67–80.
[3] A.N. Hayhurst, D.B. Kittelson, and N.R. Telford, *Mass spectrometric sampling of ions from atmospheric pressure flames-II: Aerodynamic disturbance of a flame by the sampling system*, Combust. Flame 28 (1977), pp. 123–135.
[4] A.N. Hayhurst and D.B. Kittelson, *Mass spectrometric sampling of ions from atmospheric pressure flames-III: Boundary layer and other cooling of the sample*, Combust. Flame 28 (1977), pp. 137–143.
[5] V.V. Dubinin, B.Ya. Kolesnikov, and G.I. Ksandopulo, *Correction of probe sampling in flames*, Combust. Explo. Shock 13 (1977), pp. 785–788.
[6] O.I. Smith, *Probe-induced distortions in the sampling of one-dimensional flames*, Combust. Flame 40 (1981), pp. 187–199.

[7] A.C. Yi and E.L. Knuth, *Probe-induced concentration distortions in molecular beam mass-spectrometer sampling*, Combust. Flame 63 (1986), pp. 369–379.

[8] S.D.T. Axford and A.N. Hayhurst, *The effects of applied electric fields on the mass spectrometric sampling of ions in atmospheric-pressure flames*, Proc. Combust. Inst. 23 (1990), pp. 363–370.

[9] O.P. Korobeinichev, *The use of mass spectrometry to study the structure of flames and combustion processes*, Russ. Chem. Rev. 49 (1980), pp. 497–508.

[10] S. Yoon and E.L. Knuth, *Experimental study of probe-induced distortions in molecular-beam. Mass-spectrometer sampling from flames*, Rarefied Gas Dynamics, Prog. Astronaut. Aeronaut. 74 (1981), pp. 867–881.

[11] A.T. Hartlieb, B. Atakan, and K. Kohse-Höinghaus, *Effects of a sampling quartz nozzle on the flame structure of a fuel-rich low-pressure propene flame*, Combust. Flame 121 (2000), pp. 610–624.

[12] J.C. Biordi, C.P. Lazarra, and J.F. Papp, *Molecular-beam mass-spectrometry applied to determine the kinetics of reactions in flames*, Combust. Flame 23 (1974), pp. 73–82.

[13] P. Desgroux, L. Gasnot, J.F. Pauwels, and L.R. Sochet, *Correction of LIF temperature measurements for laser absorption and fluorescence trapping in a flame*, Appl. Phys. B (1995), pp. 401–407.

[14] U. Struckmeier, P. Obwald, T. Kasper, L. Böhling, M. Heusing, M. Köhler, A. Brockhinke, and K. Kohse-Höinghaus, *Sampling probe influences on temperature and species concentrations in molecular beam mass spectroscopic investigations of flat premixed low-pressure flames*, Z. Phys. Chem. 223 (2009), pp. 503–537.

[15] O.P. Korobeinichev, A.G. Tereshchenko, I.D. Emel'yanov, A.L. Rudnitskii, S.Yu. Fedorov, L.V. Kuibida, and V.V. Lotov, *Substantiation of the probe mass-spectrometric method for studying the structure of flames with narrow combustion zones*, Combust. Explo. Shock 21 (1985), pp. 524–530.

[16] D. Stepowski, D. Puechberty, and M.J. Cottereau, *Use of laser-induces fluorescence of OH to study the perturbation of a flame by a probe*, Proc. Combust. Inst. 18 (1981), pp. 1657–1573.

[17] I.D. Emel'yanov, O.P. Korobeinichev, A.G. Tereshchenko, and L.V. Kuibida, *Heat transfer between flame and probe in mass-spectrometric research on flame structure*, Combust. Explo. Shock 22 (1986), pp. 168–175.

[18] R.M. Fristrom and A.A. Westenberg, *Flame Structure*, McGraw-Hill, New York, 1965.

[19] E.W. Kaiser, T.J. Wallington, M.D. Hurley, J. Platz, H.J. Curran, W.J. Pitz, and S.K. Westbrook, *Experimental and modeling study of premixed atmospheric-pressure dimethyl ether − air flames*, J. Phys. Chem. A 104 (2000), pp. 8194–8206.

[20] M.F.M. Nogueira and E.M. Fisher, *Effects of dimethyl methylphosphonate on premixed methane flames*, Combust. Flame 132 (2003), pp. 352–363.

[21] O.I. Smith and D.W. Chandler, *An experimental study of probe distortion to the structure of one-dimensional flames*, Combust. Flame 63 (1986), pp. 19–29.

[22] J.A. Green and T.M. Sugden, *Some observations on the mechanism of ionization in flames containing hydrocarbons*, Proc. Combust. Inst. 9 (1963), pp. 607–621.

[23] N.A. Burdett and A.N. Hayhurst, *Hydration of gas phase ions and the measurement of boundary layer cooling during flame sampling into a mass spectrometer*, J. Chem. Soc. Faraday Trans. I. 78 (1982), pp. 2997–3007.

[24] A.N. Hayhurst and N.R. Telford, *The occurrence of chemical reactions in supersonic expansions of a gas into a vacuum and its relation to mass spectrometric sampling*, Proc. Roy. Soc. London A. 322 (1971), pp. 483–507.

[25] M. Musick, P.J. Van Tiggelen, and J. Vandooren, *Experimental study of the structure of several fuel-rich premixed flames of methane, oxygen, and argon*, Combust. Flame 105 (1996), pp. 433–450.

[26] C. Douté, J.L. Delfau, R. Akrich, and C. Vovelle, *Experimental study of the chemical structure of low-pressure premixed n-heptane-O2-Ar and iso-octane-O2-Ar flames*, Combust. Sci. Technol. 124 (1997), pp. 249–276.

[27] C. Vovelle, J.-L. Delfau, and L. Pillier, *Laminar hydrocarbon flame structure*, Combust. Explo. Shock 45 (2009), pp. 365–382.

[28] E. Bastin, J.-L. Delfau, M. Reuillon, C. Vovelle, and J. Warnatz, *Experimental and computational investigation of the structure of a sooting C_2H_2-O_2-Ar flame*, Proc. Combust. Inst. 22 (1989), pp. 313–322.

[29] A. Lucassen, N. Labbe, P.R. Westmoreland, and K. Kohse-Höinghaus, *Combustion chemistry and fuel-nitrogen conversion in a laminar premixed flame of morpholine as a model biofuel*, Combust. Flame. 158 (2011), pp. 1647–1666.
[30] P. Obwald, K. Kohse-Hoinghaus, U. Struckmeier, T. Zeuch, L. Seidel, L. Leon, and F. Mauss, *Combustion chemistry of the butane isomers in premixed low-pressure flames*, Z. Phys. Chem. 225 (2011), pp. 1029–1054.
[31] A.G. Shmakov, O.P. Korobeinichev, I.V. Rybitskaya, A.A. Chernov, D.A. Knyazkov, T.A. Bolshova, and A.A. Konnov, *Formation and consumption of NO in H_2+O_2+N_2 flames doped with NO or NH_3 at atmospheric pressure*, Combust. Flame 157 (2010), pp. 556–565.
[32] O.P. Korobeinichev, V.M. Shvartsberg, S.B. Ilyin, A.A. Chernov, and T.A. Bolshova, *Laminar flame structure in a low-pressure premixed $H_2/O_2/Ar$ mixture*, Combust. Explo. Shock 35 (1999), pp. 239–244.
[33] I.E. Gerasimov, D.A. Knyazkov, S.A. Yakimov, T.A. Bolshova, A.G. Shmakov, and O.P. Korobeinichev, *Structure of atmospheric-pressure fuel-rich premixed ethylene flame with and without ethanol*, Combust. Flame 159 (2012), pp. 1840–1850.
[34] O.P. Korobeinichev, S.B. Ilyin, V.M. Mokrushin, and A.G. Shmakov, *Destruction chemistry of dimethyl methylphosphonate in $H_2/O_2/Ar$ flame studied by molecular beam mass spectrometry*, Combust. Sci. Technol. 116 (1996), pp. 51–67.
[35] O.P. Korobeinichev, S.B. Ilyin, V.M. Shvartsberg, and A.A. Chernov, *The destruction chemistry of organophosphorus compounds in flames—I: Quantitative determination of final phosphorus-containing species in hydrogen-oxygen flames*, Combust. Flame 118 (1999), pp. 718–726.
[36] R.J. Kee, J.F. Grcar, M.D. Smooke, and J.A. Miller, *A program for modeling steady, laminar, one-dimensional premixed flames*, Report No. SAND85-8240, Sandia National Laboratories, 1985.
[37] R.J. Kee, F.M. Rupley, and J.A. Miller, *Chemkin-II: A Fortran chemical kinetics package for the analysis of gas phase chemical kinetics*, Report No. SAND89-8009B, Sandia National Laboratories, 1989.
[38] G.P. Smith, D.M. Golden, M. Frenklach, N.W. Moriarty, B. Eiteneer, M. Goldenberg, C.T. Bowman, R.K. Hanson, S. Song, W.C. Gardiner, Jr., V.V. Lissianski, and Z. Qin, *GRI-Mech 3.0* (2009) http://www.me.berkeley.edu/gri_mech/
[39] N.N. Yanenko, *The Method of Fractional Steps for Solving Multi-Dimensional Problems of Mathematical Physics in Several Variables*, Springer-Verlag, Berlin, 1971.
[40] F.H. Harlow and J.E. Welsh, *Numerical calculation of time-dependent viscous incompressible flow of fluid with free surface*, Phys. Fluids 8 (1965), pp. 2182–2189.
[41] A.G. Tereshchenko, O.P. Korobeinichev, P.A. Skovorodko, A.A. Paletsky, and E.N. Volkov, *Probe method for sampling solid-propellant combustion products at temperatures and pressures typical of a rocket combustion chamber*, Combust. Explo. Shock 38 (2002), pp. 81–91.
[42] A. Broc, S. De Benedictis, G. Dilecce, M. Vigliotti, R.G. Sharafutdinov, and P.A. Skovorodko, *Experimental and numerical investigation of an O_2/NO supersonic free jet expansion*, J. Fluid Mech. 500 (2004), pp. 211–237.
[43] J.O. Hirschfelder, Ch.F. Curtiss, and R.B. Bird, *Molecular Theory of Gases and Liquids*, Wiley, New York, 1954.
[44] P.A. Skovorodko, A.G. Tereshchenko, D.A. Knyazkov, O.P. Korobeinichev, and A.A. Paletsky, *Experimental and numerical study of thermocouple-induced perturbations of the methane flame structure*, Combust. Flame 159 (2012), pp. 1009–1015.
[45] W.E. Kaskan, *The dependence of flame temperature on mass burning velocity*, Proc. Combust. Inst. 6 (1956), pp. 134–143.
[46] H.Y. Wong, *Handbook of Essential Formulae and Data on Heat Transfer for Engineers*, Longman, London, New York, 1977.
[47] Yu.V. Polezhaev and F.B. Yurevich, *Thermal Protection* (Teplovaya zashchita), [in Russian] Energiya, Moscow, 1976.